Some Effects of the Wind on Rings

WILLIAM K. DEWAR

Department of Oceanography and the Supercomputer Computations Research Institute, Florida State University, Tallahassee, FL 32306

GLENN R. FLIERL

Department of Earth, Atmospheric and Planetary Science, MIT, Cambridge, MA 02139

(Manuscript received 13 November 1986, in final form 21 April 1987)

ABSTRACT

Some simple air–sea momentum transfer models, which include sea surface velocity and temperature, are considered for their effects on Gulf Stream rings. Perturbing the stress calculation with sea surface velocity results in a "top drag", which causes interior motions to decay. Numerical experiments with equivalent barotropic quasi-geostrophic dynamics and reasonable estimates for the top drag suggest that this mechanism can account for a significant fraction of observed isotherm subsidence rates in rings. Perturbing the stress calculation with a temperature sensitive drag coefficient produces a dipolar Ekman pumping field over a ring. For an eastward directed wind, the result is a tendency for the ring to self-propagate to the south. Integral constraints can be used to estimate the meridional propagation rate precisely, and for reasonable stress and thermal anomaly values, the estimate compares well with observations.

1. Introduction

It is known from boundary layer meteorology that the coupling between the ocean and the atmosphere at the ocean surface is a function of sea surface state (Charnock, 1981). For example, the net momentum transferred from the atmosphere to the ocean at the surface of the ocean depends on the wind speed relative to the water, and is smaller for a given wind speed where the water is flowing with the wind rather than against it. It is also known that there is an enhanced momentum exchange between the atmosphere and the ocean if the ocean is warm relative to the air. The explanation for this thermal dependence of stress involves the development of a convectively turbulent boundary layer in the atmosphere. Other factors, like oceanic wave state, can also affect momentum transfer. In many cases, oceanic effects are weak compared to atmospheric effects and it is sensible to neglect the variations in the ocean surface structure when computing air–sea fluxes. Several of the phenomena of current interest to physical oceanographers (e.g., jets and eddies) are, however, characterized by significant gradients in surface structure, which can significantly influence atmospheric exchange.

One example of such an effect involves the surface temperature distribution in the North Atlantic. The sea surface temperature in the North Atlantic on the scales of the general circulation varies by several degrees, and the gradients in temperature are intensified on the western boundary by the Gulf Stream. This variation in surface temperature structure can alter the wind stress field near the Gulf Stream (by the thermal mechanism mentioned above) to a shape which can maintain the Gulf Stream jet structure in the deep water (Bunker, 1976). Thus, Behringer, et al. (1979) suggested by studying a model with temperature feedback on stress that a jetlike eastward Gulf Stream extension is a result of heat transport by the general circulation. Huynh and Veronis (1981) examined other aspects of temperature dependence in the calculation of stress.

Gulf Stream rings are another example of oceanic phenomena characterized by extreme variations in their surface properties. Typical ring surface speeds are on the order of (100–200) cm s^{-1} and vary in direction by 180° over roughly (200–300) km (the Ring Group, 1981; Joyce and Kennelly, 1985). Similarly, surface temperature variations across rings can easily be (5–6)°C (Schmitt and Olson, 1985; Dewar, 1986). It therefore seems likely that rings will modify the air–sea exchange processes in their vicinity, and one would expect the evolution of rings to reflect this.

In the present paper, some simple analytical and numerical models of wind-forced Gulf Stream rings are examined with two objectives in mind. First, we will discuss how wind stress will be affected by the presence of a ring and how forced ring behavior will differ from that of an unforced ring. Second, we will attempt to quantify the effects of the forcing on rings and make comparisons with observations. The main results of our analysis are that the decay and motion of oceanic rings are likely to be influenced by the interaction of wind and ring surface structure.

a. Background

This paper considers two different models of ring–atmosphere interaction and is divided into two sections. The studies most relevant to both parts are the numerical studies of coherent vortices conducted by McWilliams and Flierl (1979), who used a quasi-geostrophic model, and Mied and Lindemann (1979), who used a shallow water model. Two other less related studies of the interactions of wind and ocean vortices were conducted by Stern (1965, 1966).

Relative to the first model discussed in this paper, both McWilliams and Flierl and Mied and Lindemann found that wave radiation in their models was a function of vortex strength, and that the energy loss due to radiation from vortices as strong as Gulf Stream rings was of secondary importance. McWilliams and Flierl found that 79% of the main vortex decay in their equivalent barotropic calculation was accounted for by nonradiative effects, the most important of these being biharmonic friction. Wave radiation was somewhat more important in their two layer calculations, because of the presence of the barotropic mode, but friction still dominated. Mied and Lindemann reported a similar dependence of their results on friction. At the least, these calculations suggest the importance of modeling dissipative processes carefully. The biharmonic and lateral frictions used in the above studies are necessary to control the well-known enstrophy cascade, but, as the authors freely admit, are probably not good models of small-scale effects. In the first part of this paper, we demonstrate that the dependence of wind stress on the motion of the wind relative to the sea surface flow produces a drag on a ring. Indeed, the form the effect takes in the equations is very similar to a Laplacian frictional operator, with the added benefit that the "viscous" coefficient can be computed in terms of known quantities. Numerical experiments demonstrate that the decay of a ring, as measured by the subsidence of its maximum vortex isopycnal depression, is controlled by this "top drag" and proceeds at rates comparable to those observed in the field.

It was also demonstrated in McWilliams and Flierl (1979) that model warm rings tend to move south, and model cold rings north, as a result of wave radiation. The computed meridional propagation speeds were on the order of 0.5 km day^{-1}. Warm rings in the field during periods of isolated evolution are observed to drift to the south (for reasons not yet understood) at rates of a few kilometers per day, so it appears that the numerical experiments underestimate warm ring southward motion by a significant amount. The comparisons are even more problematic for cold rings, which are also observed to drift south. In this case, numerical experiments do not even predict the proper sense of ring motion. We suggest in the second part of this paper that a sizeable fraction of the observed southward motion of warm rings is in response to a connection between wind stress and ring sea surface temperature anomalies. This connection is based on the idea that cold air over warm water will be convectively turbulent, and thus transfer momentum to the ocean with greater efficiency than would a nonturbulent boundary layer. This mechanism is the same as that studied by Behringer et al. (1979) and Huynh and Veronis (1981). The forced southward ring tendencies for warm rings computed in this paper are O(1 km day^{-1}), and are as large as those driven by wave radiation. Forced meridional motion is likely to be less important for cold rings because of their weak surface temperature signatures, but is nonetheless directed to the south.

This paper is organized as follows: In the next section, we discuss the "top drag" model, which incorporates surface velocity in the calculation of wind stress. This dynamically affects the interior through the curl of the stress, and a simple formulation for the curl is derived. Numerical experiments are discussed and compared with data. In section 3, we discuss the model which includes temperature feedback on wind stress. This model is inherently nonlinear, and requires the solution of a coupled set of equations. Again, the results of numerical experiments are described and compared with observations. Section 4 contains a summary.

b. Numerical methods

We have based these models on the equivalent barotropic quasi-geostrophic equation. It has also been necessary for the model discussed in section 3 to solve an advection–diffusion equation. All the numerical solutions were performed on a doubly periodic 32 by 32 grid with a grid spacing of 20 km, and were solved using pseudospectral methods (Gottlieb and Orszag, 1977). Leapfrog time steps with an implicit formulation of the diffusion terms were used to perform most of the time integrations. An Euler time step was performed every 50th iteration to suppress the computational mode (Haltiner, 1971). Some of the model calculations performed originally by McWilliams and Flierl (1979) were repeated here, and it is worth noting that no substantive differences were found in the results of these two independently coded models.

2. The wind-forced spin down of gulf stream rings

We will model rings in this study using the equivalent barotropic quasi-geostrophic equation:

$$(\nabla^2 - \Gamma^2)\alpha_t + Q\xi J(\alpha, (\nabla^2 - \Gamma^2)\alpha) + \alpha_x = F(0)Qw_e - K\nabla^6\alpha \quad (1)$$

Equation (1) has been used in the past for the study of rings (McWilliams and Flierl, 1979) and the study of coherent vortices in general (Flierl et al., 1980). While quasi-geostrophic dynamics are limited by parametric constraints, (1) is a useful model for the examination

of the potential vorticity dynamics of vortices. We prefer to interpret (1) using the modal decomposition formalism described in Flierl (1978), in which case $\alpha(x, y, t)$ is the horizontal structure function of the first baroclinic mode, Γ^{-1} a nondimensional Rossby radius, $Q = U/\beta l^2$ a nondimensional measure of nonlinearity based on the north–south variation in the Coriolis parameter (β), a scale estimate of the fluid velocity (U), and the length scale of the ring (l), ξ a self-interaction coefficient for the first baroclinic mode (Flierl, 1978), K a biharmonic friction coefficient and W_e the surface Ekman pumping. Equation (1) has been nondimensionalized in the standard way, subscripts $[x, y, t]$ denote differentiation and ∇^2 is the Laplacian operator. The vertical structure in this model is determined by the first baroclinic eigenfunction (Flierl, 1978), which will be denoted as $F(z)$. Thus, pressure is $P = \alpha(x, y, t)F(z)$.

The stress imparted on the ocean by the wind is computed according to the bulk formula

$$\tau = \frac{\rho_a}{\rho} C_d |\mathbf{U}_a - \mathbf{u}|(\mathbf{U}_a - \mathbf{u}), \tag{2}$$

where ρ_a is the density of air, C_d an empirical drag coefficient, $\mathbf{U}_a$ wind velocity and $\mathbf{u}$ surface flow velocity. In general, the drag coefficient, C_d, is affected by many things (humidity, air temperature, water temperature, etc.). To focus here on the effects of surface velocity, we will ignore these influences and approximate C_d by the constant value:

$$C_d = 10^{-3}$$

(Charnock, 1981). Wind affects the interior potential vorticity dynamics of a quasi-geostrophic model through Ekman pumping, which is proportional to the curl of τ. For a steady eastward wind, the Ekman pumping can be written as

$$w_e = \frac{\mathbf{k} \cdot \mathrm{curl}\tau_0}{f_0} + \frac{\rho_a}{\rho_0} C_d U_a (2u_y - v_x)/f_0, \tag{3}$$

where it has been assumed that $|\mathbf{u}| \ll |U_a|$, and τ_0 denotes τ ($\mathbf{u} = 0$).

In the present model, we will assume

$$\mathbf{k} \cdot \mathrm{curl}\tau_0 = 0,$$

in order to focus as simply as possible on the effects of the surface velocity field on stress. This assumption is also reasonable. The mean winds in the open ocean vary on the scales of the basin; hence, the variation of their curl is nearly invisible on the scales of a ring.

If now the surface velocities are replaced by pressure gradients (through the geostrophic balance), (3) becomes

$$w_e = -\left[\frac{\hat{C}_d U_a F(0) L}{(UH)}\right][2\alpha_{yy} + \alpha_{xx}] = -\frac{\hat{C}_d U_a F(0) L}{UH} \tilde{\nabla}^2 \alpha, \tag{4}$$

where $\hat{C}_d = \rho_a C_d/\rho_0$, and the symbol $\tilde{\nabla}^2$ denotes the differential operator $2\partial^2/\partial y^2 + \partial^2/\partial x^2$. Note that aside from the factor of 2, the Ekman pumping formula in (4) is identical to that consistent with the inclusion of bottom drag; hence, the present effect is referred to as "top drag".

The quasi-geostrophic equation becomes

$$(\nabla^2 - \Gamma^2)\alpha_t + Q\xi J[\alpha, (\nabla^2 - \Gamma^2)\alpha] + \alpha_x = -\nu\tilde{\nabla}^2\alpha - K\nabla^6\alpha, \tag{5}$$

upon substitution with (4) and is the equation we take to model wind forced Gulf Stream ring evolution. Note that the quantity

$$\nu = \hat{C}_d F^2(0) U_a/(\beta L H)$$

appears in (5) as would a coefficient of eddy viscosity. In contrast to an eddy coefficient, whose magnitude is usually only crudely known, the preceding can easily be calculated in terms of well-known quantities. A typical nondimensional value for ν is

$$\nu = O(10^{-2}) \ll 1.$$

and is relatively small.

a. Planetary wave spin down

The effects of top drag can be conveniently studied using planetary waves. Consider the continuously stratified quasi-geostrophic equation:

$$\left[\frac{\partial}{\partial t} + QJ(P, \cdot)\right]\left[\nabla^2 P + \frac{y}{Q} + \frac{\partial}{\partial z}\frac{1}{S}\frac{\partial}{\partial z}P\right] = 0,$$

where S is a nondimensional stratification parameter, which for illustrative purposes will be taken to be constant. Top drag enters the problem through the surface boundary condition:

$$w = -\tilde{\nu}\tilde{\nabla}^2 p \quad \text{at} \quad z = 0,$$

where $\tilde{\nu} = C_d L U_a/(UH)$, while the lower boundary condition is

$$w = 0 \quad \text{at} \quad z = -1.$$

Inserting a separable solution of the form:

$$P = F(z)e^{i(kx+ly)-pt}$$

yields the vertical structure equation:

$$F_{zz} - E^2 F = 0$$

$$F_z = 0 \quad \text{at} \quad z = -1$$

$$F_z = \tilde{\nu} FSQ(k^2 + 2l^2)/p \quad \text{at} \quad z = 0,$$

where $E^2 = S(k^2 + l^2 + ik/p)$. Applying the boundary conditions yields:

$$E \tanh(E) = S\tilde{\nu}Q(k^2 + 2l^2)/p,$$

which can be solved by considering a perturbation ex-

pansion for E in powers of the small parameter $\tilde{\nu}$. At lowest order in $\tilde{\nu}$, the standard planetary wave dispersion relation is obtained:

$$E_{0,n} = 0, in\pi,$$

where the subscript 0 denotes the lowest member in the perturbation sequence for E, and the n denotes the nth planetary wave mode. The next order yields:

$$E_{1,n} = QS(k^2 + 2l^2)/[(p_{0,n})(E_{0,n})], \quad n > 0$$

while the $n = 0$ solution is recovered at $O(\tilde{\nu}^{1/2})$:

$$E_{1,0} = [QS(k^2 + 2l^2)/p_{0,0}]^{1/2}.$$

In both cases, $p_{1,n}$ is positive:

$$p_{1,n} = 2Q(k^2 + 2l^2)/(k^2 + l^2 + (n\pi)^2/S), \quad n > 0$$

$$p_{1,0} = Q(2l^2 + k^2)/(k^2 + l^2)$$

indicating exponential decay.

b. Ring spindown

Given both the strength of Gulf Stream rings, and the nonlinear character of (5), it is necessary when modeling rings to obtain solutions to (5) numerically. Note also that there are a number of parameters in (5) which will affect the numerical solutions. The parameter of most interest here is ν; therefore, we have adopted standard values for the remaining parameters:

$$Q = 5.5, \quad \Gamma^2 = 2, \quad \xi = 1.8 \quad \text{and} \quad K = 5 \times 10^{-5}.$$

The values assigned to Q, Γ^2 and ξ are the same as those of the "standard" set studied by McWilliams and Flierl (1979). They employed a value for K of 5×10^{-4}, while we have chosen a value for K which is a factor of 10 smaller. The reasons for this will become apparent. Here Γ^2 and ξ were computed using the mean MODE density profile. Thus, a value of 2 for Γ^2 implies a length scale of 60 km. $Q = 5.5$ is consistent with a velocity scale of 34 cm s^{-1}. [Recall that within the modal decomposition, this scale applies to the depth where $F(z) = 1$. The velocity scale appropriate to the surface involves $F(0)$, which is roughly 3. Therefore, the surface velocity scale is approximately 100 cm s^{-1}]. The ν involves the wind speed U_a in its definition and will be varied in the present numerical experiments.

c. Numerical results

Contour plots of the streamfunction α from a typical numerical solution to (5) are presented in Fig. 1. The ring is forced by the wind in this experiment; U_a was assigned the value 7 m s^{-1} ($\nu = 2.1 \times 10^{-2}$). The initial ring structure was chosen to be a Gaussian:

$$\alpha(t = 0) = e^{-r^2}$$

and is shown in (a). The streamfunction at later times, specifically days 50 and 75, are shown in (b) and (c), respectively. The "ring" stands out in these experiments as the largest amplitude signal in the streamfunction field. It remains essentially radially symmetric throughout its lifetime, although important nearby asymmetries are generated, and a field of radiated Rossby waves is developed. Comparing days 50 and 75 shows that the ring drifts to the southwest; the speed of this motion is roughly 2.5 km day^{-1}. The structure of the pressure distributions in Fig. 1 are essentially indistinguishable from those computed by McWilliams and Flierl (1979, cf. their Fig. 1), although their solutions included no effects from wind forcing (i.e., $U_a = 0$ in their calculations). Indeed, several quantitative measures of forced model evolution, such as the path of the ring (defined to be the motion of the central pressure extreme), are virtually identical to those computed using unforced results. This may be understood by computing the "center of mass" motion of the forced ring from (5). The center of mass is defined by

$$\mathbf{X} = (X, Y) = \int\int_{-\infty}^{\infty} (x, y)\alpha dA \Big/ \int\int \alpha dA$$

and evolves according to:

$$X_t = -1/\Gamma^2$$

$$Y_t = 0.$$

The above equations are identical to those which apply to unforced ring evolution and are independent of "top drag". Thus, it is no surprise that the inclusion of top drag has little effect on ring motion. On the other hand, significant effects on the evolution of the streamfunction amplitude are noted in the forced experiment. This is demonstrated in Fig. 2, where the maximum pressure amplitudes computed from a forced experiment and a free experiment are compared. The wind speed in the forced experiment was assigned the value $U_a = 14$ m s^{-1}. In both experiments K was set to 5×10^{-5}. Note that the amplitude in the forced experiment declines at better than twice the rate of the free experiment.

d. A comparison of the trends

The relative importance of the various dynamic effects in these experiments can be determined from the numerical data. For example, the amplitude decay tendencies driven by the biharmonic friction and top drag are compared in Fig. 3. The tendency due to biharmonic friction is defined as

$$(\alpha_{\text{dif}})_t = -(\nabla^2 - \Gamma^2)^{-1} K \nabla^6 \alpha$$

(see Fig. 3.a), and the decay tendency driven by the Ekman pumping is defined as

$$(\alpha_f)_t = (\nabla^2 - \Gamma^2)^{-1} F(0) Q w_e \qquad (6)$$

(see Fig. 3.b). Near ring center, $(\alpha_f)_t$ is approximately an order of magnitude greater than $(\alpha_{\text{dif}})_t$ (-0.009 compared to -0.001 at ring center). $(\alpha_f)_t$ and $(\alpha_{\text{dif}})_t$

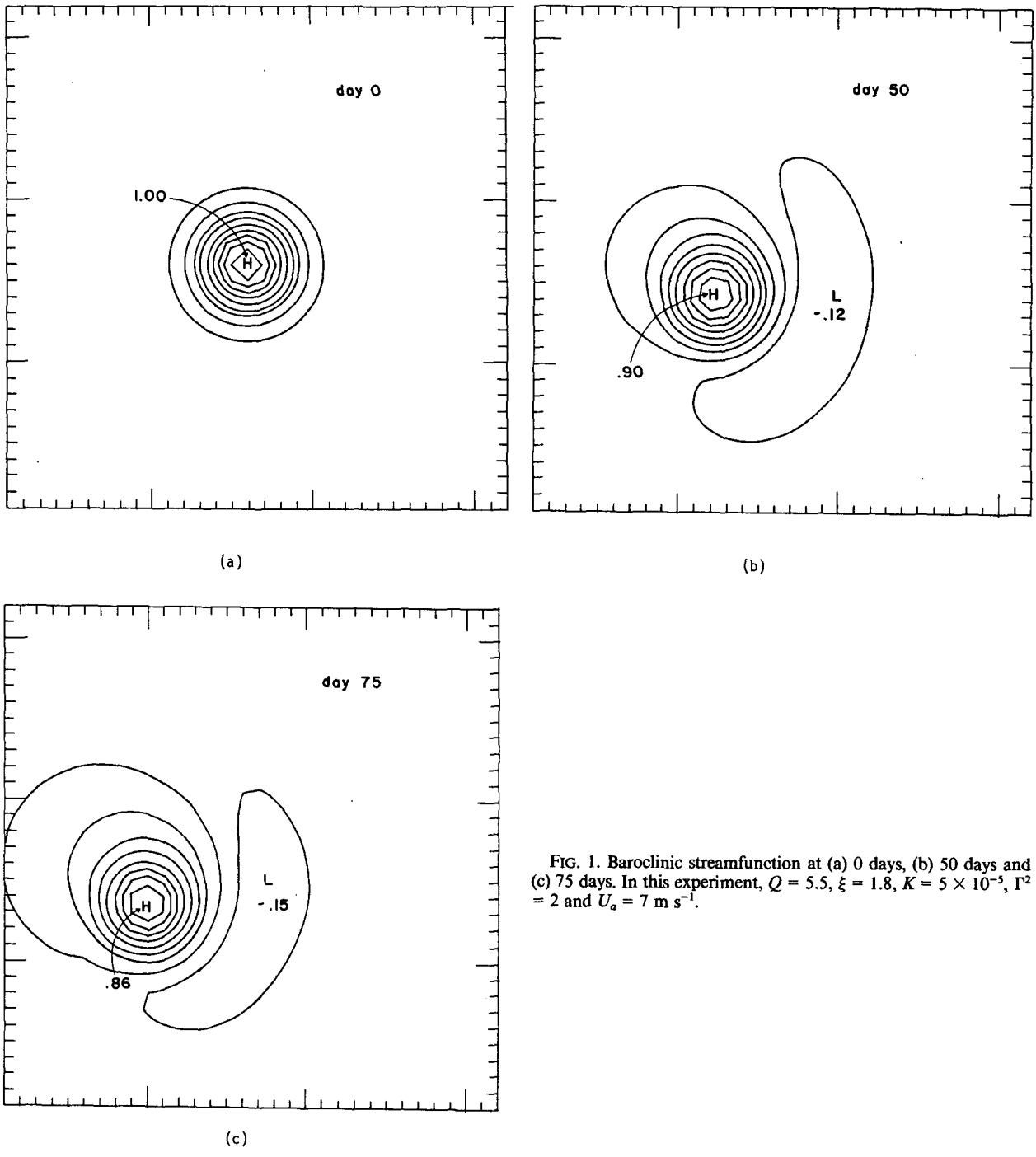

FIG. 1. Baroclinic streamfunction at (a) 0 days, (b) 50 days and (c) 75 days. In this experiment, $Q = 5.5$, $\xi = 1.8$, $K = 5 \times 10^{-5}$, $\Gamma^2 = 2$ and $U_a = 7$ m s^{-1}.

obtain more comparable values away from ring center, although $(\alpha_f)_t$ is generally larger than $(\alpha_{\text{dif}})_t$. Note, however, that decay is substantially weaker away from ring center than at ring center. The magnitudes of the nonconservative effects at ring center are compared as functions of time in Fig. 4, from which it is evident that $(\alpha_f)_t$ dominates $(\alpha_{\text{dif}})_t$ throughout the experiment. Consequently, we conclude that the decay driven by biharmonic friction when $K = 5 \times 10^{-5}$ is of secondary importance and that the dominant nonconservative process is top drag. Similar results apply when K is elevated to 5×10^{-4}, although the amplitude decay at ring center driven by friction increases to O(40%) of that due to top drag.

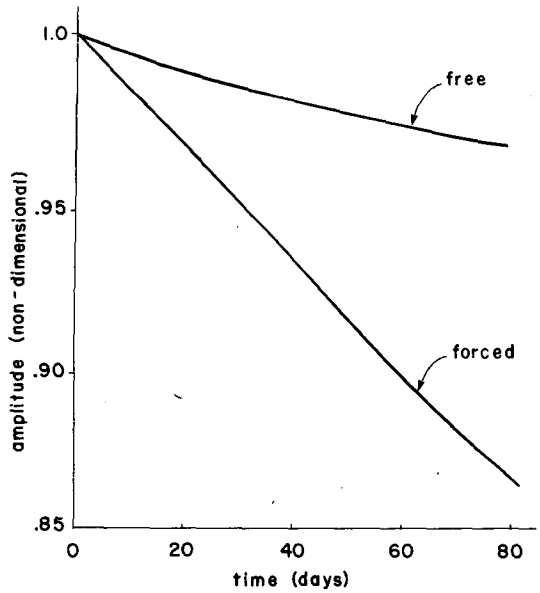

FIG. 2. Forced and unforced ring decay. Here we compare the central pressure maximum as computed from the quasigeostrophic model, with and without top drag, as a function of time. Note that in the forced experiment, the decay is roughly 2.5 times faster than in the free experiment.

Finally, forced decay may be compared to that caused by all processes, including advection and dispersion. The total trend in amplitude is defined as

$$(\alpha_a)_t = (\nabla^2 - \Gamma^2)^{-1}[-Q\xi J(\alpha, \nabla^2\alpha) - \alpha_x - K\nabla^6\alpha - \nu\tilde{\nabla}^2\alpha],$$

an example of which is plotted Fig. 3c. Note that away from ring center, advection and dispersion dominate, producing trends which overwhelm the nonconservative effects. Near ring center, however, the sum of these effects goes through a zero crossing, leaving only the nonconservative effects. Thus near ring center, the effect of top drag can be O(90%) of the total trend.

Several experiments with different combinations of K and ν have been conducted in order to explore a range of likely parameter settings. The results are summarized in Table 1. The numbers quoted there reflect the decay rates measured at ring center, and have been converted to isopycnal subsidence rates using the quasigeostrophic formula:

$$d = -F_z(z)\alpha(x, y, t)/N,$$

where d is the displacement of an isopycnal from its resting depth; F_z and N^2 were evaluated from the MODE data at a depth corresponding to the 17°C isotherm. Note all values in Table 1 are in tens of centimeters per day. For comparison, Parker (1971) suggested that cold ring isotherm anomalies subside at 50 cm day^{-1}, while warm core rings apparently relax at rates closer to 100 cm day^{-1} (Olson et al., 1985). In either case, it appears that top drag can account for a significant fraction of the observed subsidence rates, which recommends top drag as a viable candidate mechanism for the decay of rings in the real ocean.

e. Effects on potential vorticity

The wind forcing affects the mass balance of the layer under the Ekman layer through pumping. This in turn affects the interior dynamically through relative vorticity generation and thermocline deformation. It is of interest to compute the relative magnitudes of these two quantities. Specifically, the forced generation of potential vorticity is

$$q_t = (\nabla^2 - \Gamma^2)(\alpha)_t = F(0)Qw_e$$

where $\nabla^2\alpha_t$ measures the creation of relative vorticity and $-\Gamma^2\alpha_t$ the tendency of the thermocline to deform. Inverting the above equation, [see (6)], yields the deformation effect, $-\Gamma^2(\alpha_f)_t$, which may then be used to compute the relative vorticity tendency. Maps of both quantities are presented in Fig. 5, from which it is seen that the relative vorticity tendency is O(3–5) times larger than the deformation tendency. Similar results apply if Γ^2 is allowed to vary between 1 and 4, which covers the length scales typically thought to apply to rings.

These results show that the vertical velocity at the base of the Ekman layer is greater than the vertical velocity at the thermocline. For an anticyclone, mass balance then requires radially inward directed secondary velocities in the upper layer, so one might paradoxically find a tendency for subsurface material outside a warm ring to drift inward in spite of a rising thermocline. Note that such secondary flow generates positive relative vorticity and is consistent with ring spin down.

3. Southward ring propagation forced by sea surface temperature

In this section, we compute the effect of a temperature sensitive coefficient of drag on the evolution of a ring. Again, we consider the equivalent barotropic quasigeostrophic model in (1) as the basic model, and again wind stress is computed according to (2). In this section, however, in order to focus on the effects of temperature dependence in the stress calculation, $\hat{C}_d$ will be considered as a function of surface buoyancy (b) and the effect on τ of u, the surface flow, will be ignored. The results of the last section demonstrate that including u in (Z) causes ring decay. This will be modeled in these experiments by using a larger value for K than was used in the previous section, namely $K = 5 \times 10^{-4}$. This corresponds to the biharmonic coefficient used by McWilliams and Flierl (1979).

We shall use

$$\hat{C}_d(b) = \hat{C}_d(b_0) + \frac{\partial \hat{C}_d}{\partial b}(b - b_0),$$

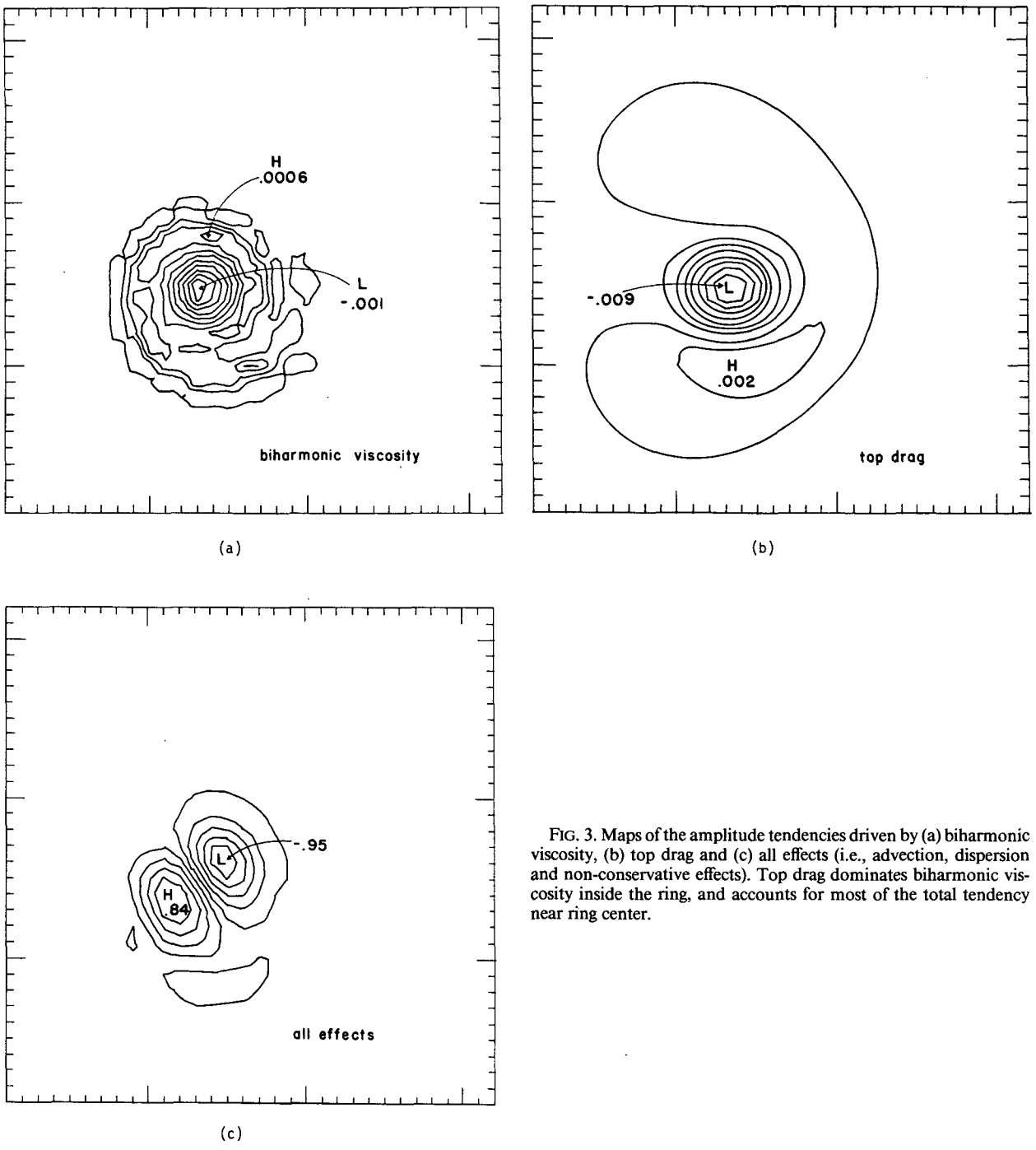

FIG. 3. Maps of the amplitude tendencies driven by (a) biharmonic viscosity, (b) top drag and (c) all effects (i.e., advection, dispersion and non-conservative effects). Top drag dominates biharmonic viscosity inside the ring, and accounts for most of the total tendency near ring center.

where b_0 is a reference buoyancy and $\partial \hat{C}_d/\partial b$ is constant, as a model of a temperature sensitive drag coefficient. Inserting this in the formula for Ekman pumping yields

$$W_e = \frac{1}{f_0}\mathbf{k}\cdot\operatorname{curl}\underset{\sim}{\tau} = \frac{1}{f_0}\hat{C}_d k\cdot\operatorname{curl}(|\mathbf{U}_a|\mathbf{U}_a) - \frac{\hat{C}'_d}{f_0}\mathbf{k}\cdot\underset{\sim}{\tau}_0\times\nabla b,$$

where $\hat{C}'_d$ is the fractional rate of change of the drag coefficient with respect to buoyancy:

$$\hat{C}'_d = \frac{1}{\hat{C}_d(b_0)}\frac{\partial \hat{C}_d}{\partial b},$$

and $\underset{\sim}{\tau}_0 = \underset{\sim}{\tau}(b = b_0)$. For the purposes of the present calculations, we will assume the wind is directed uniformly to the east, thus:

$$W_e = -\frac{1}{f_0}\tau_0\hat{C}'_d\frac{\partial b}{\partial y}.$$

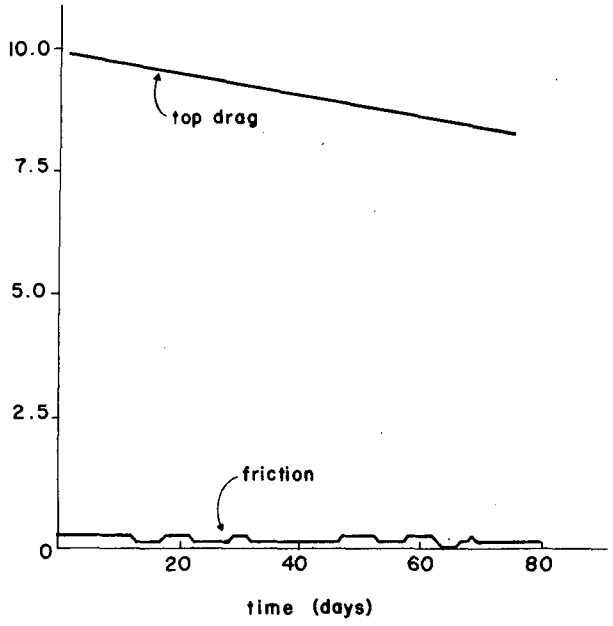

FIG. 4. Comparison in time of the amplitude tendencies driven by biharmonic friction and top drag. The nondimensional amplitude, plotted on the vertical axis, has been been multiplied by 10^3. Note top drag is always substantially greater in effect than is viscosity.

Note, the calculation of the Ekman pumping now requires the prediction of the sea surface buoyancy distribution. The prognostic equation for the surface buoyancy, which closes the system, will be taken as

$$\frac{\partial}{\partial t}b + ub_x + vb_y = K_b\nabla^2 b + \mathcal{F},$$

where u and b are evaluated at $z = 0$ and $\mathcal{F}$ is some net surface buoyancy forcing, such as would be computed by a mixed layer model; K_b is an eddy diffusion coefficient for buoyancy.

a. Analytical and numerical results

If the wind is directed uniformly to the east, the coupled set of equations describing ring evolution is

$$(\nabla^2 - \Gamma^2)\alpha_t + Q\xi J(\alpha, \nabla^2\alpha) + \alpha_x = \kappa b_y - K\nabla^6\alpha \quad (7a)$$

$$b_t + QF(0)J(\alpha, b) = K_b\nabla^2 b + \mathcal{F}, \quad (7b)$$

where $\kappa = -F(0)\hat{C}'_d\tau_0 b_0/(\beta LUH)$ in which τ_0 is a scale estimate of the wind stress variations (1 dyn cm^{-2}), b_0 a scale estimate of the surface buoyancy variations (1 cm s^{-2}), $F(0)$ is the surface value of the first baroclinic eigenfunction and is computed to be 3 from the MODE data, and H is an estimate of the total fluid depth (5 km).

It is possible to anticipate the effects of a temperature dependent drag on interior motions by analytically computing the motion of the center of mass, defined as

$$\mathbf{X} = (X, Y) = \int_{-\infty}^{\infty}\int (x, y)\alpha dA \Big/ \int\int \alpha dA.$$

Upon integration, (7) yield (assuming α and b vanish at infinity):

$$X_t = -1/\Gamma^2 \quad (8a)$$

$$Y_t = \frac{\kappa}{\Gamma^2}\int\int bdA \Big/ \left(\int\int \alpha dA\right) \quad (8b)$$

which, to the extent that the ring remains coherent, track ring motion. The computed movement of the zonal component of the center of mass is identical to that of the unforced case, while the net southward center of mass drift, which vanishes for an unforced ring, is here non zero and obviously a result of the forcing.

The sense of the forced meridional drift is determined by the ratio of the average surface buoyancy anomaly to the average pressure anomaly. κ is negative, so both a warm pool overlying a high pressure center and a cold pool overlying low pressure result in a southward drift of the center of mass. This is noteworthy as the former describes warm core rings and the latter cold core rings. A temperature sensitive drag coefficient in conjunction with eastward wind pushes both to the south.

Further, by averaging both (7.a) and (7.b), we obtain

$$\left[\int\int bdA\right]_t = \int\int \mathcal{F}dA$$

$$\left[\int\int \alpha dA\right]_t = 0,$$

so, the meridional center of mass motion can be computed from the initial conditions and some knowledge of the heat fluxes. If, for example, $\mathcal{F} = 0$:

TABLE 1. Subsidence rates. The biharmonic coefficients used in the parameter study are listed across the top of the chart, and the values of U_a are listed down the side. The dashes (—) denote the lack of an experiment at this parameter setting. Three different values of Γ^2 have also been tested. The listed subsidence rates are in cm day^{-1}, and the U_a are in m s^{-1}. All subsidence rates are O (10s of cm day^{-1}).

	K		
u_a	5×10^{-8}	5×10^{-5}	5×10^{-4}
($\Gamma^2 = 2$)			
0	16	18	30
7	30	43	50
14	—	50	61
($\Gamma^2 = 1$)			
14	—	70	—
($\Gamma^2 = 1$)			
14	—	35	—

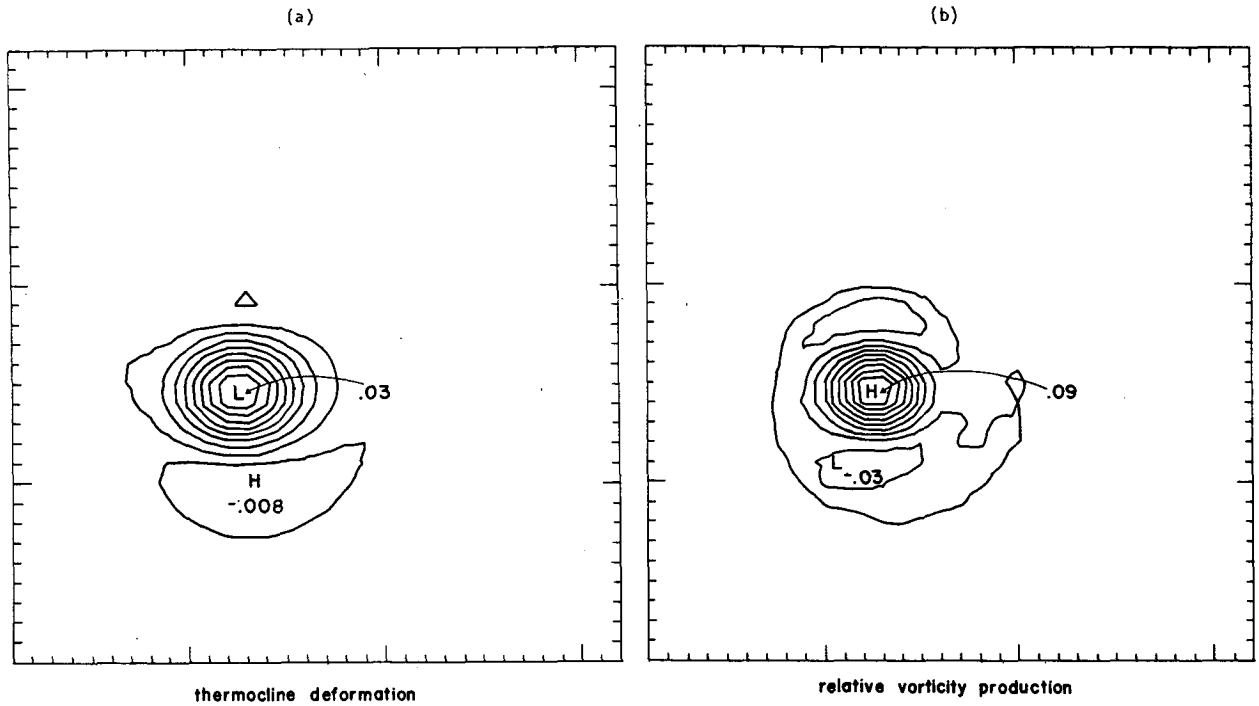

FIG. 5. Potential vorticity tendencies. The thermocline deformation tendency is shown in (a) and relative vorticity generation in (b). Comparison shows relative vorticity generation is dominant; thus, for a warm ring, a mass influx is required in the upper layer.

$$Y_t = \frac{\kappa}{\Gamma^2} \cdot \frac{\iint b(t=0)dA}{\iint \alpha(t=0)dA} = \frac{l_b^2 \kappa}{l^2 \Gamma^2}, \tag{9}$$

where we have assumed initial Gaussian fields:

$$b(t=0) = e^{-r^2/l_b^2}$$

$$\alpha(t=0) = e^{-r^2/l^2}$$

for both α and b.

Note, in the more general case, where $\mathcal{F} \neq 0$, variations in Y_t will arise in accord with the change in the surface anomaly. Thus, for a warm ring this model predicts that the rates of southward ring drift should be smaller during periods of weak surface temperature expression (summer) and greater during periods of strong surface temperature expression (winter). Similar effects are theoretically possible for cold rings; however, their surface signatures tend to be considerably weaker than for warm rings (Dewar, 1986).

Results of a numerical integration of (7) are presented in Fig. 6 for the case $\mathcal{F} = 0$. Here $\hat{C}'_d$ has been assigned the constant value 0.5 cm^{-1} sec^2. This accounts reasonably well, if crudely, for drag coefficient variations at modest air–sea temperature differences (cf. Bunker, 1976). This experiment is meant as a rough simulation of a warm ring during winter conditions, when surface buoyancy structure is maintained by strong convection (Schmitt and Olson, 1985; Dewar, 1986).

The surface buoyancy structure evolves as discussed in Dewar and Flierl (1985) and develops the classical "tail" structure emanating from the "stagnation" point in the flow. For reference, the temperature change across the ring is 5°C. The physical structure of the pressure field visually resembles that computed in section 2, with the evident radiative production of the two neighboring pressure centers. Amplitudes of the main vortex in these results, in which forcing is included, and those of McWilliams and Flierl (1979), in which forcing has been neglected, are essentially indistinguishable. Significant differences between the evolution of the unforced and forced rings arise, however, when the ring paths are compared (see Fig. 7). Clearly the forced ring is moving south at a greater rate (~ -1 km day^{-1}) than is the freely evolving ring (~ -0.4 km day^{-1}). l_b [see (9)] for this experiment was set to 1.5, thus:

$$Y_t = \kappa \frac{9}{8} \approx -0.6 \text{ km day}^{-1},$$

which accounts for the difference in the computed meridional motion in these experiments.

It is less apparent, but nonetheless true, that the zonal propagation of the forced ring differs from the free ring. Examining the time history of the path of the pressure maximum (see Table 2) demonstrates that the forced

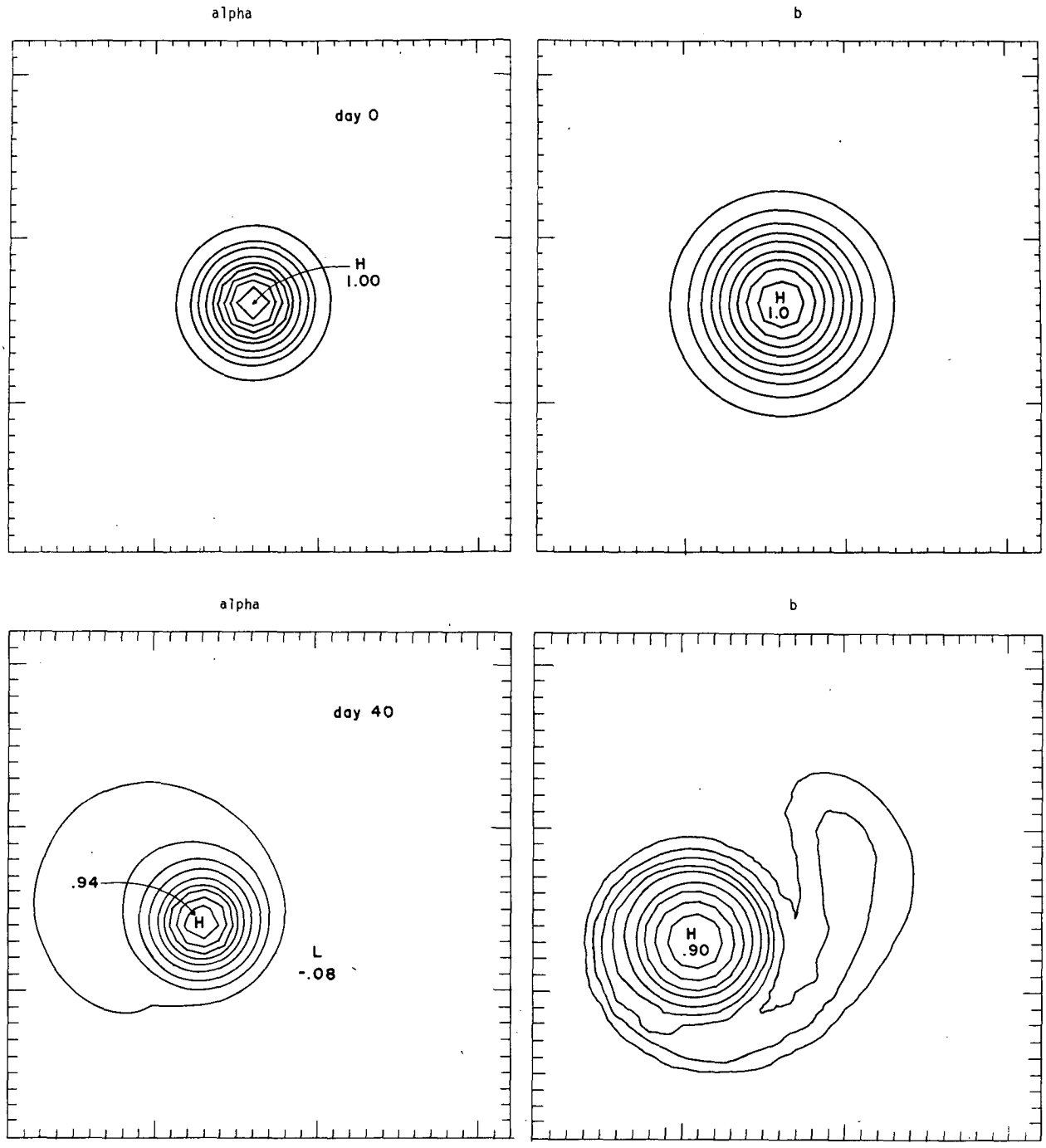

FIG. 6. Surface buoyancy and pressure maps from an experiment with a temperature dependent drag coefficient. Surface buoyancy and streamfunction are presented at 0 days in (a), 40 days in (b) and 60 days in (c). The parameters are standard and $\hat{C}'_d = 0.5$ cm^{-1} s^2. The variation in surface temperature is 5°C.

ring is moving more slowly to the west than is the free ring. This is somewhat surprising, as no differences in the zonal center of mass motion are expected from (8).

The zonal ring propagation can be understood by computing the difference between the center of mass and ring center, which by definition is

$$X - x_c = \iint (x - x_c)\alpha dA \Big/ \iint \alpha dA$$

$$Y - y_c = \iint (y - y_c)\alpha dA \Big/ \iint \alpha dA,$$

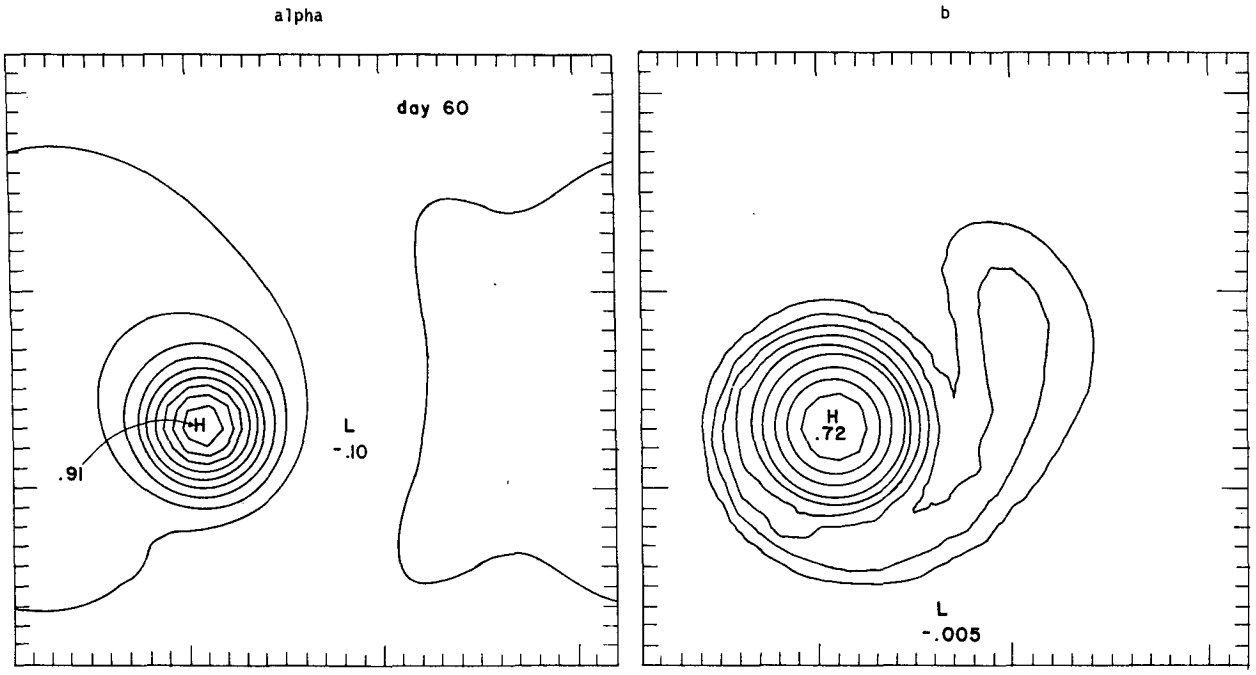

FIG. 6. (*Continued*)

where x_c denotes the location of the pressure maximum. Clearly, if α were radially symmetric, the above integrals would vanish. This suggests the importance of the nonsymmetric radiation field to ring motion. Defining the "departure field" of the ring as

$$\alpha' = \alpha - \alpha(x_c, y_c, t)e^{-(x-x_c)^2-(y-y_c)^2},$$

the above integrals become

$$X - x_c = \iint (x - x_c)\alpha' dA \Big/ \iint \alpha dA$$

$$Y - y_c = \iint (y - y_c)\alpha' dA \Big/ \iint \alpha dA.$$

Plots of α' for both the free and the forced ring are given in Fig. 8. Note the primary constituents of α' in both cases are a high pressure center and a low pressure center, which are situated west and east of (x_c, y_c), respectively. The effect on the ring of either a western high or an eastern low is to push the ring west and south. It is evident that the position of these centers relative to the ring differs between these two experiments; the centers in the forced ring experiment are rotated cyclonically from the positions of the centers in the free ring experiment. Thus, the departure field is not as effective at moving the forced ring zonally as it is in the free experiment, which accounts for the different zonal drifts. The reasons for the rotating of the departure field will be discussed shortly.

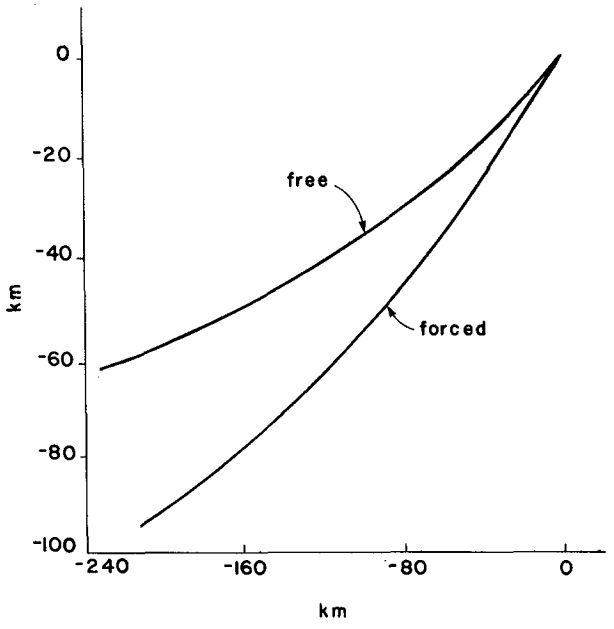

FIG. 7. The trajectory of the central extreme in pressure from a freely evolving ring experiment and an experiment with $\hat{C}_d(b)$ in which the drag coefficient varies with buoyancy. Note, the temperature dependent drag drives the ring to the south at roughly twice the rate of the free ring. Zonal propagation rates are also affected by the forcing. The paths are from an experiment of 150 days duration. Only the first 70 days of this experiment are reported in Table 2.

b. Potential vorticity considerations

The dynamic explanation for the enhanced southward drift and the displacement of the neighboring pressure centers lies in the potential vorticity balance.

TABLE 2. Locations of the local maximum of pressure versus time. All distances are in km and measured relative to initial ring center. Freely evolving and forced ring experiments are compared. Note that the meridional diplacement of the ring is greater in the forced experiment, while the zonal displacement of the ring is greater in the free experiment.

Free Evolution			Forced Evolution		
Time (days)	X_{rel} (km)	Y_{rel} (km)	Time (days)	X_{rel} (km)	Y_{rel} (km)
0.0	0.0	0.0	0.0	0.0	0.0
5.0	−4.4	−4.4	5.0	−4.4	−4.4
10.0	−13.3	−6.7	10.0	−6.7	−6.7
15.0	−17.8	−11.1	15.0	−17.8	−8.9
20.0	−26.7	−13.3	20.0	−22.2	−17.8
25.0	−35.6	−15.6	25.0	−28.9	−22.2
30.0	−51.1	−22.2	30.0	−46.7	−26.7
35.0	−55.6	−24.4	35.0	−53.2	−33.3
40.0	−66.7	−26.7	40.0	−64.4	−35.6
45.0	−82.2	−28.9	45.0	−68.9	−42.2
50.0	−95.6	−33.6	50.0	−86.7	−46.7
55.0	−105.4	−35.8	55.0	−95.6	−53.3
60.0	−115.6	−35.6	60.0	−102.2	−57.8
65.0	−122.2	−42.2	65.0	−115.6	−64.4
70.0	−137.8	−42.2	70.0	−126.7	−66.7

The potential vorticity trend forced by the Ekman pumping

$$q_t = [\nabla^2 - \Gamma^2]\alpha_t = F(0)Qw_e$$

is plotted in Fig. 9. Note that the Ekman pumping field which develops over a warm ring consists of two centers of opposing sign, consistent with the warm center being a region of locally enhanced stress. Accordingly, the Ekman layer is horizontally divergent to the north of the ring and horizontally convergent to the south of the ring. The above elliptic operator can be inverted to compute the forced deformation ($-\Gamma^2\alpha_t$) and relative vorticity ($\nabla^2\alpha_t$) tendencies, plots of which are given in Fig. 10. The character of both trends is such that they

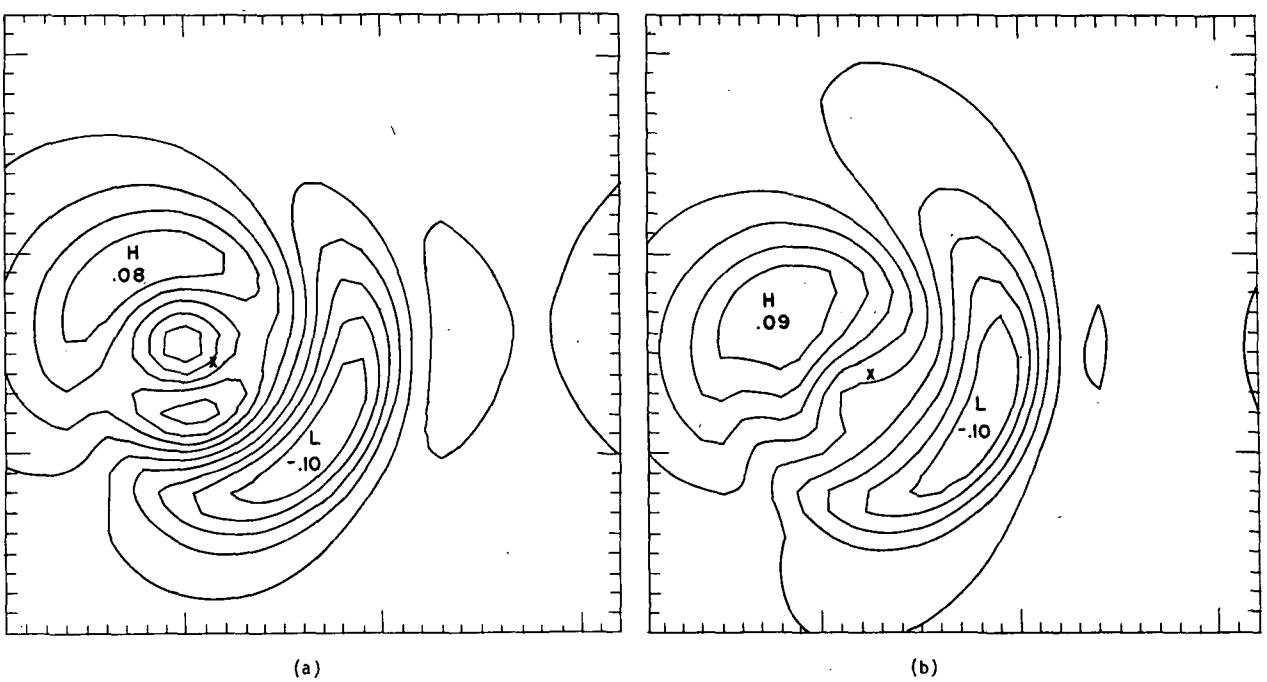

FIG. 8. Departure fields from the (a) free and (b) forced experiment are compared. The amplitudes of the major centers are comparable; however, their locations relative to the ring are different. The forcing moves the dispersion field cyclonically about the ring, thus reducing the speed at which the ring propagates zonally. The "×" symbols denote ring center.

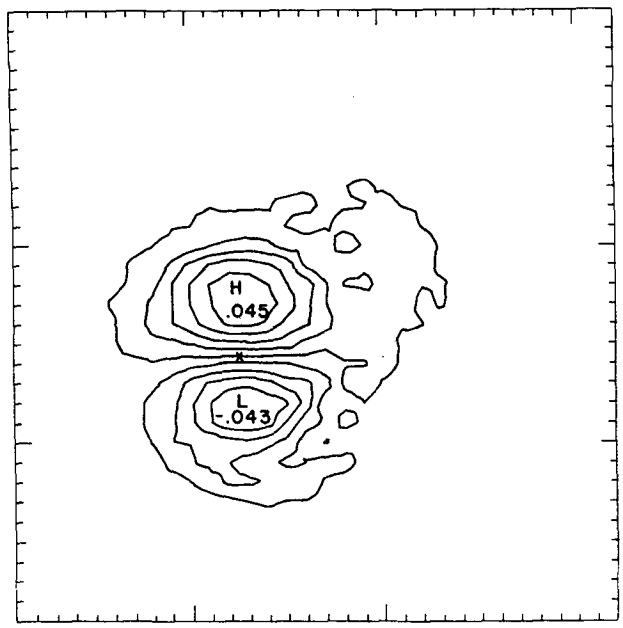

FIG. 9. Ekman pumping over a Gulf Stream ring as forced by a temperature sensitive drag coefficient. Two centers of opposite sign develop in the Ekman pumping field because of the central ring temperature anomaly. For a warm ring, the surface is horizontally divergent to the north and horizontally convergent to the south. The "×" symbol denotes ring center.

tend to move the pressure structure associated with the ring to the south. For example, the sign of the thermocline deformation term acting on the northern (southern) half of the ring is positive (negative). Thus, the northern (southern) part of the ring thermocline is lifted (depressed), which is equivalent to bodily displacing the hydrographic structure of the ring to the south. Similarly, positive (negative) relative vorticity is generated in the northern (southern) part of the ring. This decelerates (accelerates) the ring, which feeds back through geostrophy to flatten (steepen) the thermocline. The effect here is thus a dynamic movement of the ring to the south. This scenario is schematically depicted in Fig. 11.

The potential vorticity of fluid outside of the ring is also affected. Note that fluid initially west of the ring first experiences a positive trend in potential vorticity due to forcing as it begins to move anticyclonically about the ring. It therefore develops less anomalous negative relative vorticity, and the location of the leading high pressure center which develops is shifted slightly to the south. As the fluid continues around the ring, it eventually experiences a negative forced trend in its potential vorticity, thus shifting the position of the trailing low slightly to the north. Thus, the differences between the departure fields of the forced and free rings in Fig. 10 are accounted for.

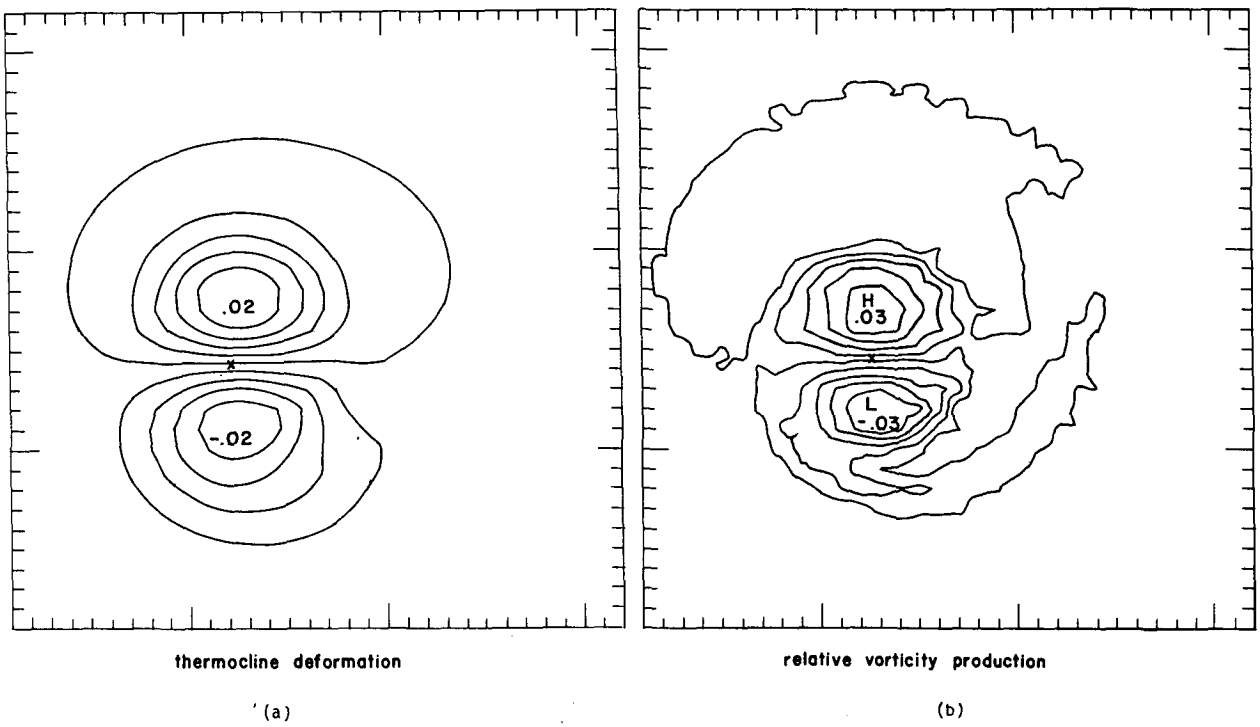

FIG. 10. Potential vorticity trends. Thermocline deformation is plotted in (a) and relative vorticity generation in (b). Both are comparable in magnitude, and both act to shift the pressure distribution to the south, as depicted in Fig. 11. The "×" symbols denote ring center.

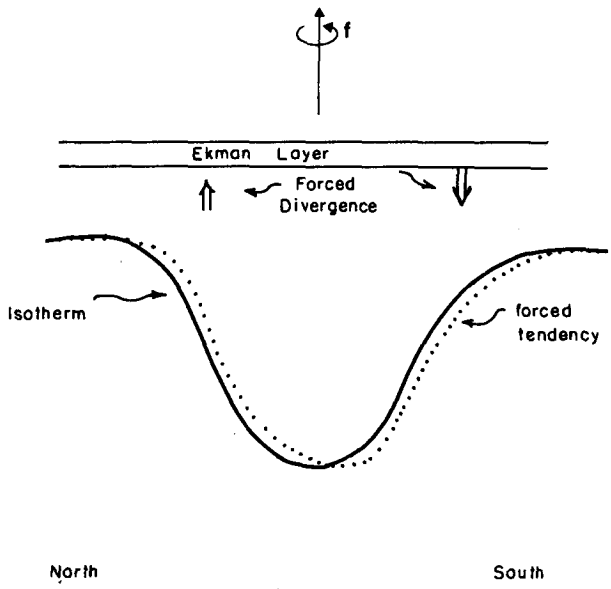

FIG. 11. Schematic depiction of forced southward propagation. The suction at the northern ring edge lifts the thermocline and generates anticyclonic vorticity. The pumping at the southern edge depresses the thermocline and generates negative relative vorticity. The resulting tenedency is a shift of the ring to the south.

4. Discussion

The coupling between atmosphere and ocean depends upon many factors, including the state of the sea surface. Gulf Stream rings are characterized by considerable surface structure in both surface velocity fields and surface temperature distributions, and should therefore locally affect the transfers of momentum between the ocean and the atmosphere. In this paper, we have extended the usual formulas for the stress imparted on the ocean by the wind to include dependences on sea surface velocity and sea surface temperature. Accordingly, we have found two important components of the evolution of strongly nonlinear, isolated quasigeostrophic vortices (which we have taken as our model of rings), i.e., their propagation and decay, to be modified by atmospheric interaction.

The dependence of wind stress on sea surface velocity results in a "top drag". An analysis based on planetary waves demonstrated that top drag will generally cause the decay of oceanic motions. It is noteworthy that Pacanowski (personal communication) finds similar results in a study of wind-driven equatorial flow. The rates computed here for isothermal subsidence in rings are comparable to observed rates, suggesting this mechanism might be important in rings. Further analysis suggested the mass fluxes associated with this top drag were balanced near the surface. For a warm ring, this suggests an influx of water to the ring beneath the mixed layer. Conclusive evidence of this type of circulation is hard to find; biological tracers tend to be dominated by in situ production rather than physical factors, and the estimated secondary velocities are weak. On the other hand, comparison of the salinity anomaly field of warm ring 82B observed in April and June, 1982 (Schmitt and Olson, 1985, their Figs. 7a and 7b) suggests qualitatively that during this period the fluid between the 10° and 15°C isotherms moved radially inward. It is known that during this period, 82B was evolving in relative isolation from the Gulf Stream and that the 10°–15°C layer was just under the mixed layer. While this is not conclusive, these data are consistent with the present calculations.

It is also worth pointing out that top drag is a physically motivated nonconservative process and, unlike biharmonic and lateral friction, depends upon a coefficient (C_d) whose magnitude is relatively well known (Charnock, 1981). In our calculations, we were able to reduce the coefficient of biharmonic friction to the point where it was having a minor affect on the decay of the large scale structure (although it was still consuming the enstrophy cascade). We can thus claim in some sense to be doing a "better job" of modeling dissipative processes than if we had used only biharmonic friction.

Including the dependence of the drag coefficient on sea surface temperature resulted in a southward drift of the main vortex. Integral constraints demonstrate that this tendency applies to both warm and cold rings, although one expects the magnitude of the effect to be substantially smaller for cold rings because of their weak sea surface temperature distribution.

The result is interesting as field observations of warm rings suggest a mean meridional motion of O(−2 km day^{-1}) during periods of isolated evolution (Brown, et al., 1986). Meridional drift rates computed from theoretical and model calculations are smaller than this by a significant amount. The numerical simulations of McWilliams and Flierl (1979), for example, suggest southward vortex migration of ~0.5 km day^{-1}, while Flierl's (1984) theoretical analysis of the evolution of a thin upper layer warm lens suggests southward drifts of O(0.1 km day^{-1}). The forced southward ring propagation computed here is O(1 km day^{-1}), which is the same magnitude as the observations. The suggestion from this analysis is that some substantial fraction (maybe as much as ½) of the observed meridional ring motion is a result of the Ekman pumping produced by a temperature sensitive drag coefficient.

Acknowledgments. The authors gratefully acknowledge the support provided by the National Science Foundation (Grant OCE-8240455) for this research. WKD is also supported by NSF Grant OCE-8415475 to the University of North Carolina. Pat Klein is thanked for typing the manuscript and Beth Raynor for producing the drawings.

REFERENCES

Behringer, D., L. Regier and H. Stommel, 1979: Thermal feedback on wind-stress as a contributing cause of the Gulf Stream. *J. Mar. Res.*, **37,** 699–709.

Brown, D., P. Cornillion, S. Emmerson and H. Carle, 1986: Gulf Stream warm core rings: a statistical study of their behavior. *Deep-Sea Res.*, **33,** 1459–1473.

Bunker, A., 1976: Computations of surface energy flux and annual air–sea interaction cycles of the North Atlantic ocean. *Mon. Wea. Rev.*, **104,** 1122–1140.

Charnock, H., 1981: Air–sea interaction, *Evolution of Physical Oceanography, Scientific Surveys in Honor of Henry Strommel,* B. Warren and C. Wunsch, Eds., MIT Press, 482–503.

Dewar, W., 1986: Mixed layers in Gulf Stream rings. *Dyn. Atmos. Oceans,* **10,** 1–29.

——, and G. Flierl, 1985: Particle trajectories and simple models of transport in coherent vortices. *Dyn. Atmos. Oceans,* **9,** 215–252.

Flierl, G., 1978: Models of vertical structure and the calibration of two-layer models. *Dyn. Atmos. Oceans,* **2,** 341–381.

——, 1984: Rossby wave radiation from a strongly nonlinear warm eddy. *J. Phys. Oceanogr.*, **14,** 47–58.

——, V. Larichev, J. McWilliams and G. Reznick, 1980: The dynamics of baroclinic and barotropic solitary eddies. *Dyn. Atmos. Oceans,* **5,** 1–41.

Gottlieb, D., and S. Orszag, 1977: *Numerical Analysis of Spectral Methods: Theory and Applications,* BMS-NSF Monogr No. 26, S.I.A.M., 172 pp.

Haltiner, G., 1971: *Numerical Weather Prediction,* Wiley and Sons, 317 pp.

Huynh, Q., and G. Veronis, 1981: The effect of temperature-dependent exchange coefficients on poleward heat flux by oceanic gyres. *Dyn. Atmos. Oceans,* **6,** 49–66.

Joyce, T., and M. Kennelly, 1985: Upper ocean velocity structure of Gulf Stream warm core ring 82B. *J. Geophys. Res.,* **90**(C5), 8839–8844.

McWilliams, J., and G. Flierl, 1979: On the evolution of isolated, nonlinear vortices. *J. Phys. Oceanogr.*, **9,** 1155–1182.

Mied, R., and G. Lindemann, 1979: The propagation and evolution of cyclonic Gulf Stream rings. *J. Phys. Oceanogr.*, **9,** 1183–1206.

Olson, D., R. Schmitt, M. Kennelly and T. Joyce, 1985: A two-layer diagnostic model of the long-term physical evolution of warm core ring 82B. *J. Geophys. Res.,* **90**(C5), 8813–8822.

Parker, C., 1971: Gulf Stream rings in the Sargasso Sea. *Deep-Sea Res.*, **18,** 981–993.

Ring Group, the, 1981: Gulf Stream cold core rings: Their physics, chemistry and biology. *Science,* **212,** 1091–1100.

Schmitt, R., and D. Olson, 1985: Wintertime convection in warm-core rings: Thermocline ventilation and the formation of mesoscale lenses. *J. Geophys. Res.*, **90,** C5, 8823–8838.

Stern, M., 1965: Interaction of a uniform windstress with a geostrophic vortex. *Deep-Sea Res.*, **12,** 355–367.

——, 1966: Interaction of a uniform wind stress with hydrostatic eddies. *Deep-Sea Res.*, **13,** 193–203.